Research Article

Contrast enhancement for images in turbid water

HUIMIN LU,[1,2,3,*] YUJIE LI,[1] LIFENG ZHANG,[1] AND SEIICHI SERIKAWA[1]

[1]Department of Electronic and Electrical Engineering, Kyushu Institute of Technology, Kitakyushu 8048550, Japan
[2]State Key Laboratory of Ocean Engineering, Shanghai Jiaotong University, Shanghai 200240, China
[3]State Key Laboratory of Marine Geology, Tongji University, Shanghai 200092, China
*Corresponding author: luhuimin@ieee.org

Absorption, scattering, and color distortion are three major degradation factors in underwater optical imaging. Light rays are absorbed while passing through water, and absorption rates depend on the wavelength of the light. Scattering is caused by large suspended particles, which are always observed in an underwater environment. Color distortion occurs because the attenuation ratio is inversely proportional to the wavelength of light when light passes through a unit length in water. Consequently, underwater images are dark, low contrast, and dominated by a bluish tone. In this paper, we propose a novel underwater imaging model that compensates for the attenuation discrepancy along the propagation path. In addition, we develop a robust color lines-based ambient light estimator and a locally adaptive filtering algorithm for enhancing underwater images in shallow oceans. Furthermore, we propose a spectral characteristic-based color correction algorithm to recover the distorted color. The enhanced images have a reasonable noise level after the illumination compensation in the dark regions, and demonstrate an improved global contrast by which the finest details and edges are enhanced significantly.   © 2015 Optical Society of America

OCIS codes: (100.2980) Image enhancement; (110.0113) Imaging through turbid media.

http://dx.doi.org/10.1364/JOSAA.32.000886

1. INTRODUCTION

Currently, autonomous underwater vehicles (AUVs) and remotely operated vehicles (ROVs) are commonly used for underwater object recognition. In the past two decades, sonar has been widely used to detect and recognize objects in underwater environments. However, for short-range object recognition, vision sensors must be used instead of sonar because sonar yields low-quality images [1].

In underwater observation, large suspended particles in turbid water cause scattering. The underwater optical images thus suffer from poor visibility because of the medium. Additionally, color distortion occurs because different wavelengths are attenuated to different degrees in water. Consequently, captured images of underwater environments are dominated by a bluish tone. The absorption of light in water substantially reduces its intensity. In fact, objects at distances of more than 10 m from the camera are almost indistinguishable [2].

Research in this field has long focused on color correction and descattering methods. Schettini and Corchs [2] reviewed methods for image enhancement and restoration, as well as subjective and quantitative assessment indices. Integrated color models were proposed for hyper-spectral correction in [3]. These models typically involve multi-step approaches that use color histogram stretching and color correction to account

for varying depths and the use of natural or artificial lighting. Distance-based contrast and color degradation models have recently been generated for turbidity images to recover underwater scenes [4–7].

In this paper, we focus on a single image enhancement method. Single image enhancement is a challenging, but ill-posed problem. The obtained brightness of each pixel depends on the observed scene point radiance, scattering, attenuation, and ambient illumination. In reviewing recent studies, we found that research related to underwater image enhancement can be classified into the following six main categories.

(1) **Polarization**: Schechner and Karpel [8] restored images taken at significantly varied scene distances by using a polarization filter attached to a camera. A distance map of the scene was obtained by capturing two polarized images from different angles. Liang et al. [9] proposed a Stokes matrix-based four-angle rotation polarization filter to remove haze. However, these methods cannot attenuate the transmission of radiance through polarization filters or multiple exposures, especially for time variations that are adverse to visibility and illumination conditions.

(2) **Turbidity medium**: Narasimhan and Nayar [10] and Cozman and Krotkov [11] analyzed a static scene by obtaining multiple images under different visibility conditions. Although they reported impressive results, a static camera and a

significant change in media turbidity were required under constant illumination conditions.

(3) **Multi-lighting**: Narasimham *et al.* [4] and Tsiotsios *et al.* [12] proposed the use of multiple lights to estimate the backscatter from a scene. Treibitz and Schechner [13] proposed fusing images obtained using two-directional illumination to create a single clearer image. However, it is difficult to recover the time variations adverse to visibility in the presence of floating turbidity sediments.

(4) **Scene depth**: Studies have calculated scene depth to solve the ambiguities in the visibility enhancement problem [14,15]. These works made assumptions about the scene that necessitate either manual inputs or special structures. Generating this information is difficult in water.

(5) **Fusion**: Ancuti *et al.* [16] combined the Laplacian contrast, contrast, saliency, and exposure features of white-balanced and color-corrected images. They then utilized the exposure fusion algorithm to obtain the final result. However, several results were color shifted because of the exposure process; selecting the exposed images is difficult.

(6) **Prior**: Fattal [17] estimated scene radiance and derived a transmission image using single-image statistics. He *et al.* [18] analyzed numerous natural sky images and determined that most color images contain a dark channel. On the basis of this finding, they proposed a dark channel prior dehazing algorithm. The subsequent image enhancement resulted in regional contrast stretching that could cause halos or aliasing. Moreover, the dark channel assumption is based on natural outdoor image statics that might not hold in arbitrary underwater scenes.

In underwater environments, captured images are significantly influenced by the medium [19]. In the present paper, we propose a novel shallow ocean imaging model and a corresponding enhancement algorithm. First, we propose a robust color line to estimate the ambient light. Next, we estimate the transmission through an underwater median dark channel prior (UMDCP). After that, we develop a locally adaptive cross filter (LACF) to remove the scatter. Finally, color correction is performed according to the spectral properties.

2. UNDERWATER LIGHT PROPAGATION MODEL

Artificial and atmospheric light are sources of illumination in a shallow ocean environment. Suppose the intensity of light at point x is W. The illumination can be formulated using the energy attenuation model as follows:

$$E_W^c(x) = E_L^c(x) + E_A^c(x), \qquad c \in \{r, g, b\}, \qquad (1)$$

where $E_W^c(x)$ is the amount of illumination, $E_A^c(x)$ is the amount of illumination of atmospheric light at point x, $E_L^c(x)$ is the illumination of artificial light at point x, and N_{rer} is the normalized residual energy ratio [20]. In turbid water, N_{rer} has the following values:

$$N_{\mathrm{rer}}(c) = \begin{cases} 0.75 \sim 0.85 & \text{if } \lambda = 650 \sim 750 \, \mu m (\text{red}) \\ 0.86 \sim 0.95 & \text{if } \lambda = 490 \sim 550 \, \mu m (\text{green}) \\ 0.95 \sim 0.99 & \text{if } \lambda = 400 \sim 490 \, \mu m (\text{blue}). \end{cases} \quad (2)$$

We assume the distance between the artificial light and the object is $d(x)$, and $D(x)$ is the underwater scene depth. Absorption and scattering occur in this process. Suppose that

the light reflection rate is $\rho^c(x)$. In accordance with the Koschmieder model [21], the scene image $I^c(x)$ formed at the camera can be formulated as

$$I^c(x) = ((E_A^c(x) \cdot N_{\mathrm{rer}}(c)^{D(x)} + E_L^c(x) \cdot N_{\mathrm{rer}}(c)^{d(x)}) \cdot \rho^c(x))$$
$$\times T^c(x) + (1 - T^c(x))A^c, \qquad c \in \{r, g, b\}, \qquad (3)$$

where the inhomogeneous background A^c represents the ambient light and $T^c(x)$ is the transmission map.

Equation (3) incorporates the light scattered during propagation from the object to the camera through a distance $d(x)$ and a scene depth $D(x)$. Once the scene depth $D(x)$, homogeneous background A^c, and object–camera distance $d(x)$ are known, a clean image can be recovered.

As indicated in Eq. (3), we suppose the light $J^c(x)$ reflected from point x is

$$J^c(x) = (E_A^c(x) \cdot N_{\mathrm{rer}}(c)^{D(x)} + E_L^c(x) \cdot N_{\mathrm{rer}}(c)^{d(x)}) \cdot \rho^c(x)$$
$$c \in \{r, g, b\}. \qquad (4)$$

Then, Eq. (3) can be rewritten as

$$I^c(x) = J^c(x)T^c(x) + (1 - T^c(x))A^c, c \in \{r, g, b\}. \qquad (5)$$

The underwater image formation model in Eq. (5) takes into consideration the scattering effect, attenuation, and artificial lighting. Thus, we consider taking the UMDCP to remove the scattering. Meanwhile, we also consider the use of spectral characteristics to recover the underwater scene color. Figure 1 shows a schematic of the proposed model. To improve the image quality, we consider the processing flowchart shown in Fig. 2. In Fig. 2, we first adjust the white balance and apply a bilateral filtering-based deflicker filter. Next, we estimate the ambient light using color lines. The coarse transmission is then estimated by using UMDCP. Then, we use the proposed locally adaptive cross filter to refine the transmission. Once the transmission map is obtained, we can remove the scatter. Finally, we restore the scene color by using the proposed camera spectral characteristic-based color correction algorithm.

3. DESCATTERING AND COLOR CORRECTION

A. Robust Ambient Light Estimation

The ambient light A^c in Eq. (5) is often estimated as the brightest color in an image [16,22–24]. However, for underwater imaging, because artificial lighting and flashing are often used, some objects (e.g., flickers, highlights) are brighter than the ambient light [25]. The traditional approaches for estimating the ambient light may produce undesired results. To reliably
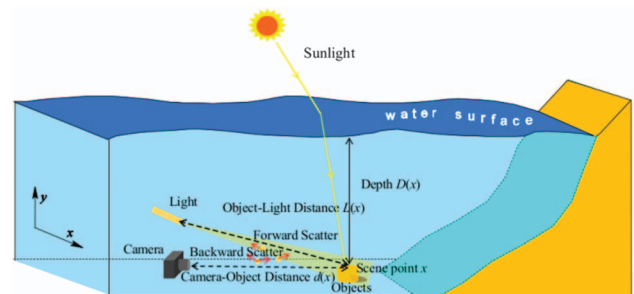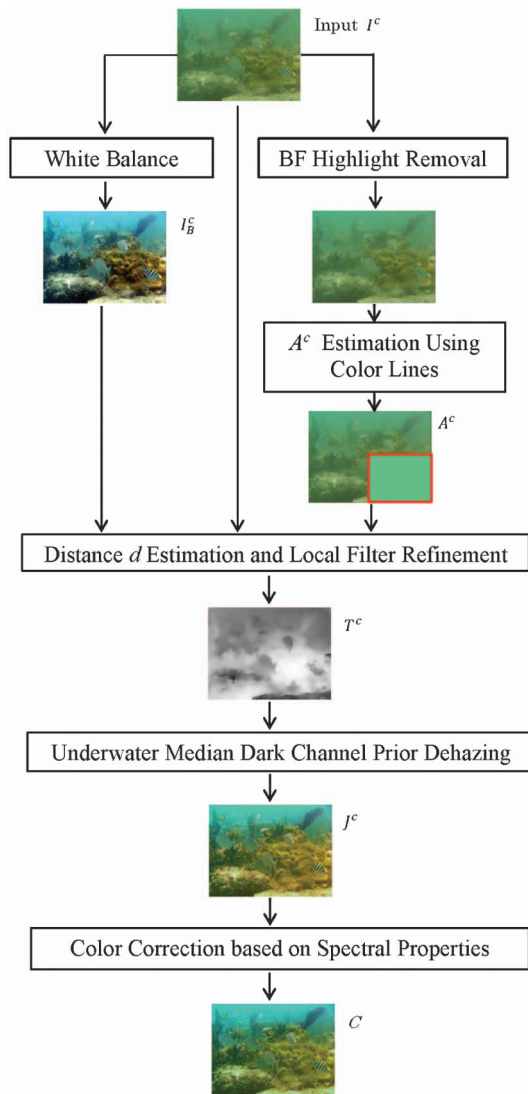

Fig. 1. Schematic of the shallow ocean imaging model.

Fig. 2. Summary of the proposed approach for underwater image enhancement.

estimate the ambient light, Kim *et al.* [26] proposed a hierarchical searching method. This method is based on quadtree subdivision. For each rectangular region, the minimum distance between the brightest pixel (255, 255, 255) and the region is estimated. This method can be used to find the brightest region in the image. However, it may also produce undesired results if the brightest pixels are objects. Fattal [27] proposed a global regularity approach based on color lines. However, in several cases, if the image contains a single surface albedo or rich details, this method results in color shifts.

To solve these problems, we propose a robust ambient light estimation method. First, we remove the highlighted regions by applying a bilateral filter-based deflicker filter. Unlike the highlight removed in [28] from specular highlights in natural scenes, the highlights we removed are with consideration for light compensation.

We first transferred the input image to SUV space. The S channel encodes the entire specular component and a fraction of the diffuse component. As the U and V channels are

functions of only the diffuse reflectance and are independent of objects, the SUV matrix is converted to a linear matrix. The color distance ρ is defined as

$$\rho = \sqrt{[I_U^c(x)]^2 + [I_V^c(x)]^2}. \tag{6}$$

The angle θ can be obtained with $I_U^c(x)$ and $I_V^c(x)$. According to the component $I_S^c(x)$ and the color distance ρ, we can remove the spatial coordinate φ. Then, we take the diffusion operation as

$$\varphi' = \max(\max(\varphi)) * BF(\max(\max(\varphi)), \theta / \max(\max(\theta))), \tag{7}$$

where BF represents the bilateral filter [29]. Finally, we can calculate the ambient light A^c using the image with highlights removed, as in [27].
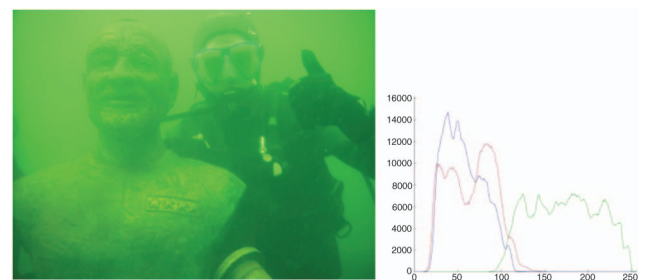
B. Coarse Transmission Estimation

According to [23], the red channel is the dark channel of underwater images. In our experiments, we found that the lowest pixel value of the RGB channels in turbid water is not always the red channel, but is occasionally the blue channel. Although the light of red wavelength is absorbed easily when it propagates in water, the distance between the camera and object is not sufficient for light of red wavelength to be significantly absorbed (Fig. 3). Additionally, the blue channel is absorbed the least. Consequently, in this paper, we use a dual channel (red and blue) to estimate the coarse transmission map.

The median filter was first proposed by Tarel and Hautiere [30] and was used for natural image dehazing. In [24], its use was extended to underwater imaging.

As previously mentioned, we found that turbid underwater images exhibited a mostly dark image $\tilde{d}(x)$. The median operation is suitable for reducing the halo effect when estimating the coarse transmission. Thus, the underwater median dark channel priors can be defined by

$$\tilde{d}(x) = \underset{\Re(m,n)}{\mathrm{median}} \left(\min_{c \in \{r,b\}} \frac{I^c(x)}{A^c} \right), \qquad c \in \{r, b\}, \tag{8}$$

where $\Re$ is a square window of size 5 × 5. For each pixel located at position (m, n) in the square patch $\Re$, the values from the red and blue channels are compared, and the lower value is selected. The proposed method can prevent the halo effect around occlusion boundaries. Accordingly, the coarse estimate of transmission is obtained using

Fig. 3. RGB histogram of an underwater image.

$$d(x) = 1 - \omega\tilde{d}(x), \tag{9}$$

where $\omega = 0.9$ for most scenes.

C. Locally Adaptive Cross Filter-Based Descattering

We roughly estimated the coarse transmission $d(x)$ in Section B. However, its transmission contains mosaic effects and yields less accurate results. Therefore, we have developed a locally adaptive cross filter to reduce the mosaic effects.

The use of a median filter has been considered an effective method for removing outliers. However, the traditional median filter usually results in morphological artifacts, such as rounded corners. To solve this problem, a weighted median filter has been proposed [31,32]. The weighted median filter can be computed from the local histograms $h(\mathbf{x}, \cdot)$ by

$$h(\mathbf{x}, i) = \sum_{\mathbf{y} \in N(\mathbf{x})} W(\mathbf{x}, \mathbf{y})\delta(V(\mathbf{y}) - i), \tag{10}$$

where $W(\cdot)$ corresponds to the weight assigned to pixel $\mathbf{y}$ inside a local window $N(\mathbf{x})$ centered at the corresponding pixel x, i is the discrete bin index (usually $i = 16$), and δ is the Kronecker delta function. The weight $W(\mathbf{x}, \mathbf{y})$ depends on the image $\mathbf{x}$, which can differ from the pixel value V. Consider it to be instead $\mathbf{x}$ by coarse transmission $d(x)$; $\mathbf{y}$ is the white-balanced image $I_B^c(x)$. Finally, the refined transmission is produced by

$$h(d(x), i) = \sum_{x \in N(x)} W(d(x), I_B^c(x))\delta(V(I_B^c(x)) - i), \tag{11}$$

where $W(\cdot)$ is the normalized convolution domain filter (NCDF) [33]. For the uniform discretization $D(\Omega)$ of the original domain Ω, NCDF can be written as

$$W(x') = (1/K_{x'}) \sum_{x \in D(\Omega)} d(x)H(t(d(\hat{x}')), t(I_B^c(\hat{x}))), \tag{12}$$

where $K_{x'} = \sum_{x \in D(\Omega)} H(t(d(\hat{x}')), t(I_B^c(\hat{x})))$ is a normalization factor for x', and $t(\cdot\prime) = ct(\cdot)$. t represents the isometric transform, and $ct(\cdot)$ is a domain transform [33]. Using the efficient moving average approach to apply normalized convolution with a box filter, the box kernel is

$$H(t(d(\hat{x}')), t(I_B^c(\hat{x}))) = \delta_B\{|t(d(\hat{x}')) - t(I_B^c(\hat{x}))| \leq r\}, \tag{13}$$

where $r = \sigma_H \sqrt{3}$ is the filter radius, δ_B is a Boolean function that equals 1 when its argument is true and 0 otherwise, and σ_H is the standard deviation of the coarse transmission map.

Finally, once the transmission $d(x)$ is known in Eq. (11), the transmission map $T^c(x)$ is dependent on the extinction coefficient β of the medium as

$$T^c(x) = e^{-\beta d(x)}. \tag{14}$$

The descattered image $J^c(x)$ can be obtained by Eq. (5),

$$J^c(x) = \frac{I^c(x) - (1 - T^c(x))A^c}{\max\{T^c(x), \varepsilon\}}, \tag{15}$$

where the definition $\varepsilon = 0.001$ is given to prevent division by 0.

D. Absorption Compensation

In Section C, we obtained the transmission map $T^\lambda(x)$ and the descattered image $J^c(x)$. To remove absorption effects, we must

obtain the reflectivity $\rho^c(x)$. For this, we take the least squares solution,

$$\rho^c(x) = (J^c(x)^T \cdot J^c(x))^{-1} \cdot J^c(x)^T$$
$$\cdot (E_A^c(x) \cdot N_{\mathrm{rer}}(c)^{D(x)} + E_J^c(x) \cdot N_{\mathrm{rer}}(c)^{d(x)}). \tag{16}$$

After removing the effects of ambient light and increasing the distance $d(x)$ between the object and the camera, the scattering can be removed by subtracting the artificial light term in Eq. (4), since our goal is to obtain $E_A^c(x) \cdot N_{\mathrm{rer}}(c)^{D(x)}$ in Eq. (4). In actual imaging, we can obtain the depth $D(x)$ using a pressure sensor. Thus, we can recover the absorption recovered image using Eq. (3).

E. Color Correction

A simple color correction method was proposed in [23]. In practice, the spectral response function of a camera also affects the colors. In this paper, we use the chromatic transfer function τ_λ to measure the light from the surface to a given object depth as

$$\tau_\lambda = \frac{E_\lambda^S}{E_\lambda^U}, \tag{17}$$

where the transfer function τ_λ at wavelength λ is derived from the irradiance of the surface E_λ^s using the irradiance of the underwater object E_λ^U. On the basis of the spectral response of the RGB camera, we convert the transfer function to the RGB domain as

$$\tau_{\mathrm{RGB}} = \int_{\lambda=400 \text{ nm}}^{750 \text{ nm}} \tau_\lambda \cdot S_c(\lambda), c \in \{r, g, b\}, \tag{18}$$

where τ_{RGB} is the weighted RGB transfer function and $Sc(\lambda)$ is the continuous underwater spectral characteristic function for color band c. Suppose the nonabsorption image is $\hat{C}(x) = E_A^c(x) \cdot N_{\mathrm{rer}}(c)^{D(x)}$. Finally, the corrected image is obtained from the weighted RGB transfer function using

$$C(x) = \hat{C}(x) \cdot \tau_{\mathrm{RGB}}, \tag{19}$$

where $C(x)$ is the color-corrected image.

4. EXPERIMENTAL RESULTS

Thirty underwater images were selected, including 15 images from the Internet and 15 images from our water tank experiments. The water tank contains 180 L water (90 cm × 45 cm× 45 cm). Both the underwater lights (INON LEs) and the underwater camera (OLYMPUS μ*Tough* TG2) were placed in the water. The objects were placed 30 cm deep. The distance between the objects and the camera was approximately 60 cm. We executed the proposed algorithm on the selected images. The performance of the proposed algorithm is evaluated both analytically and experimentally by using ground truths. We also compare the proposed method with other currently proposed state-of-the-art methods. The results demonstrate that the proposed method shows superior scatter removal and color correction capabilities.

As the first evaluation, the performance of the proposed method is compared with other methods in terms of the ability to remove scatter in water. Figure 4 illustrates the results of descattering an example image using different methods. The

method proposed by He *et al.* [22] produces a result comparable to our proposed method in regions with heavy scatter. However, the use of Laplacian matting to overcome increases in depth is time consuming. Furthermore, in this method, the ambient light is simply calculated as 0.1% of the brightness of the brightest pixels, which led the resulting images to contain some hazes.

The method proposed by Tarel and Hautiere [30] is a filter-based approach that estimates the veil by applying a median filter. The merit of this method is its linear complexity, which can be implemented in real time. However, it also tends to underestimate the transmission and produce an oversaturated result.

The double Wiener filtering-based approach proposed by Gibson *et al.* [24] can automatically refine the transmission using a locally adaptive Wiener filter. This method can also be implemented in real time. However, it estimates the ambient light using a dark channel prior, which may produce

an undesirable result. The resulting image also contains some scatter and color shifts.

Fattal [27] proposed the color line-based method can better estimate the ambient light. However, several cases show that overestimated ambient light will cause color shifts. Because of incorrectly estimating the ambient light, the result in Fig. 4(e) is the darkest. As illustrated in the zoomed-in resulting images shown in Figs. 4(g)–4(k), the proposed method demonstrates the best performance of all the methods. Less scatter and fewer halos remain when using the proposed method. Moreover, the proposed method tends to more clearly represent object details. The methods proposed by He *et al.* and Tarel *et al.* do not correctly estimate the transmission; the method proposed by Fattal *et al.* overestimates the transmission; and the method proposed by Gibson *et al.* method causes transmission jumps. As shown in Figs. 4(l)–4(p), our transmission is much clearer than those of the other methods.
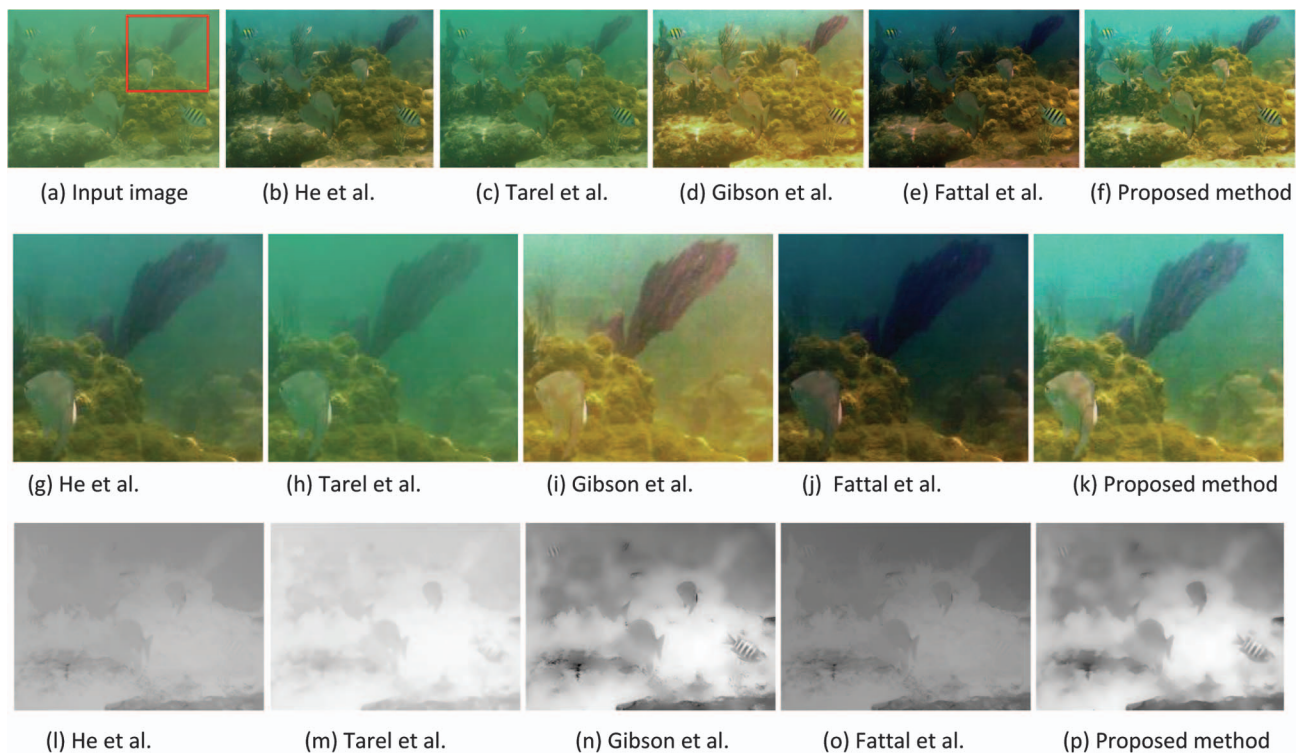
Fig. 4. Comparison of the presently proposed method with methods proposed by He *et al.*, Tarel *et al.*, Gibson *et al.*, and Fattal *et al.* (a) Input image. (b)–(f) Results of methods by He *et al.*, Tarel *et al.*, Gibson *et al.*, and Fattal *et al.*; and results of the proposed method. (g)–(k) Zoomed-in images of results shown in (b)–(f), respectively. (l)–(p) Transmission used in methods depicted in (b)–(f), respectively.
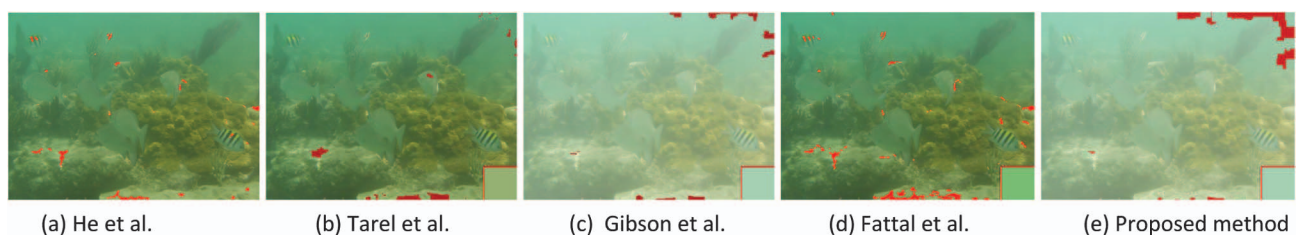

Fig. 5. Comparison of ambient light areas estimated using methods proposed by He *et al.*, Tarel *et al.*, Gibson *et al.*, Fattal *et al.*, and that of the presently proposed method.

In Fig. 5, we illustrate the estimated ambient light areas of the image with different methods. The estimated ambient light of the methods proposed by He *et al.*, Tarel *et al.*, Fattal *et al.*, and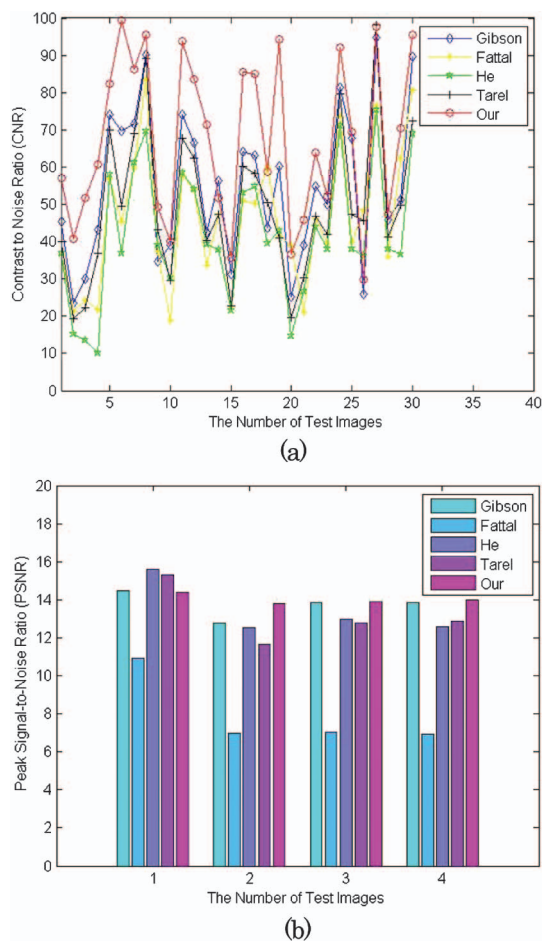 Gibson *et al.* appear unsatisfactory. Some of the objects (e.g., fish, coral reefs) are estimated to be ambient light. In contrast, because our proposed method initially removes the highlighting effect, the desired ambient light can be correctly estimated.
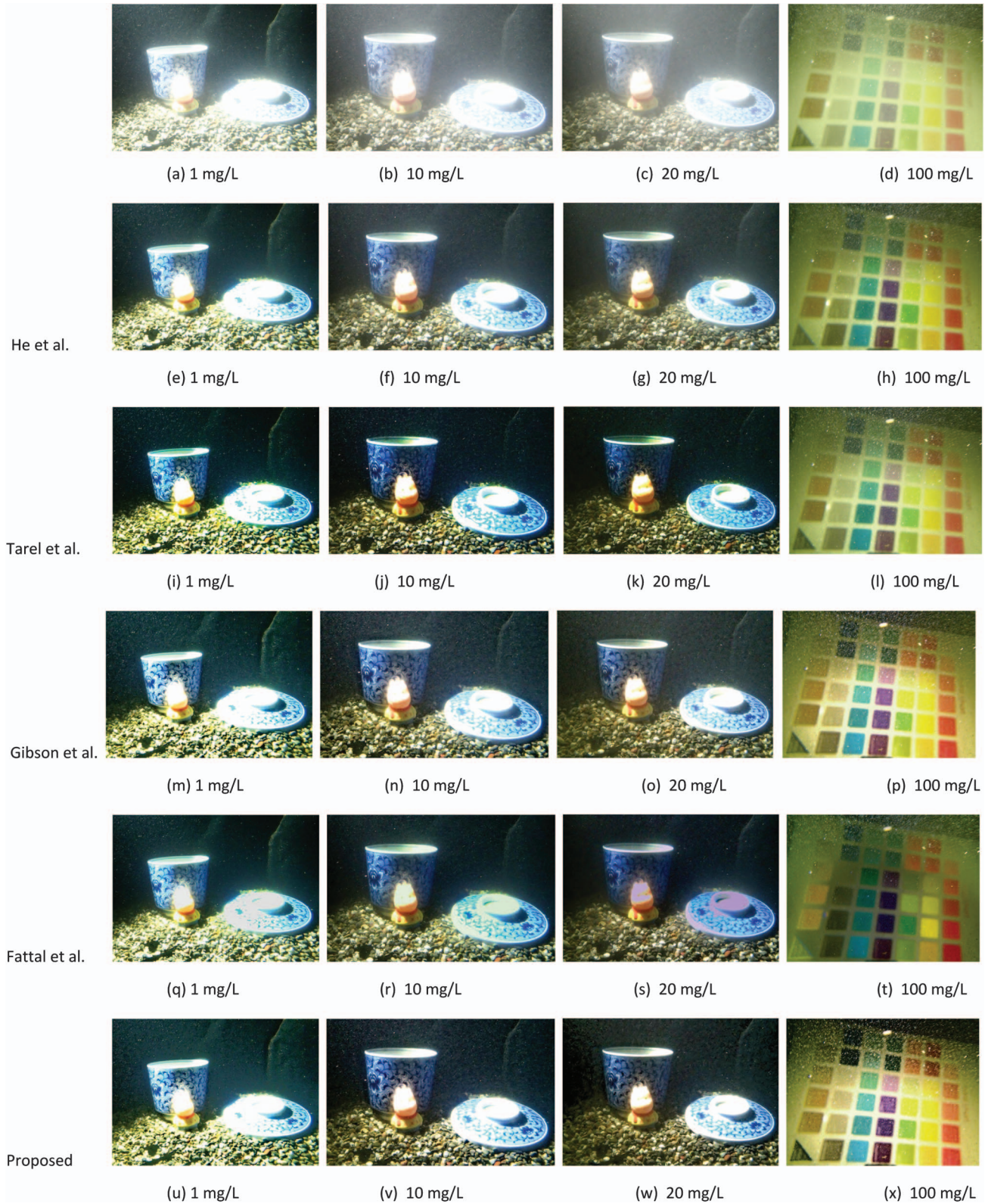
Fig. 6. Toys and cups. (a)–(d) Input images. Results with methods proposed by (e)–(h) He *et al.*, (i)–(l) Tarel *et al.*, (m)–(p) Gibson *et al.*, and (q)–(t) Fattal *et al.*; and (u)–(x) with the presently proposed method.

Figure 6 illustrates the simulation results obtained using the different methods. In this experiment, we made a linear scale of eight turbidity steps ranging from clean to heavily scattered by adding deep sea soil to the seawater (from 0.6 to 100 mg/L). Some haze remained in the resulting images using the methods proposed by He *et al.* and Gibson *et al.*, while those using the method proposed by Tarel *et al.* and Fattal *et al.* show color distortion. As shown in Figs. 6(u)–6(x), our method effectively removes haze and correctly recovers color.

In addition to visual analysis, we conducted a quantitative analysis, first from a statistical perspective and using the statistical parameters of the images. We calculated the contrast-to-noise ratio (CNR) [34], peak signal-to-noise ratio (PSNR), and structural similarity index (SSIM) of images obtained using each method [35]. The CNR is similar to the signal-to-noise ratio (SNR) and robust in measuring hazy images. The value of the CNR [34] is between 0 (worst) and 100 (best). The SSIM index determines the structural similarity between two images. The value of SSIM is between 0 (worst) and 1 (best). Figure 7(a) shows the CNR values of the selected 30 images obtained using the different methods. The CNR values demonstrate that our method performs better than other methods. However, in several cases, if the contrast of the objects was

Table 1. SSIM Values of Different Methods with Known Ground Truths

Method	Gibson	Fattal	He	Tarel	Proposed
Image 1	0.7280	0.6440	0.7686	0.7586	0.7713
Image 2	0.7350	0.2992	0.7400	0.6848	0.7995
Image 3	0.7467	0.2975	0.7495	0.7106	0.8152
Image 4	0.7464	0.2744	0.7367	0.7103	0.7106

small, a failed result was obtained. Figure 7(b) illustrates the PSNR values of the different methods using four images with known ground truths. The PSNR value of Image 1 is lower because of the heavy illumination, meaning the difference between the illumination of the objects and the background is very low. Table 1 lists the measured SSIM values of several images. These results indicate that our approach works well for scatter removal.

5. DISCUSSION AND CONCLUSION

In this paper, we have explored and successfully implemented novel enhancement techniques for underwater optical images. We proposed a physical underwater dark channel prior. To correctly estimate the ambient light, we develop a robust color line-based ambient light estimator. We also introduced a weighted guided domain filter to compensate for the transmission. The proposed filter has the benefits of preserving edges, removing noise, and reducing computation time. Moreover, the proposed underwater image color correction method successfully reconstructed colorful underwater images that are better than the images produced using current state-of-the-art methods. Our experiments showed that the proposed methods are suitable for underwater optical imaging.

In our experiments, we found that, as the amount of turbidity sediment increases, image contrast decreases. This may result in the inability to accurately estimate ambient light. Another issue is that the proposed method can only remove haze-like scatter. In future work, we need to design novel algorithms for large particles scatter removal.

Fig. 7. (a) Comparison of CNR values of different methods. (b) Comparison of PSNR values of different methods using four images with known ground truths.

REFERENCES

1. D. M. Kocak, F. R. Dalglcish, F. M. Caimi, and Y. Y. Schechner, "A focus on recent developments and trends in underwater imaging," Mar. Technol. Soc. J. **42**, 52–67 (2008).
2. R. Schettini and S. Corchs, "Underwater image processing: state of the art of restoration and image enhancement methods," EURASIP J. Adv. Signal Process. **2010**, 746052 (2010).

3. J. Ahlen, D. Sundgren, and E. Bengtsson, "Application of underwater hyperspectral data for color correction purposes," Pattern Recognition and Image Analysis **17**, 170–173 (2007).

4. S. Narasimhan, S. Nayar, B. Sun, and S. Koppal, "Structured light in scattering media," in *Proceedings of IEEE International Conference on Computer Vision* (IEEE, 2005), pp. 420–427.

5. H. Lu, Y. Li, and S. Serikawa, "Underwater image enhancement using guided trigonometric bilateral filter and fast automation color correction," in *Proceedings of IEEE International Conference on Image Processing* (IEEE, 2013), pp. 3412–3416.

6. A. Arnold-Bos, J. P. Malkasse, and G. Kervern, "Towards a model-free denoising of underwater optical images," in *Proceedings of IEEE Oceans* (IEEE, 2005), vol. 1, pp. 527–532.

7. D. L. Bongiorno, M. Bryson, D. G. Dansereau, and S. B. Williams, "Spectral characterization of COTS RGB cameras using a linear variable edge filter," Proc. SPIE **8660**, 86600N (2013).

8. Y. Schechner and N. Karpel, "Recovery of underwater visibility and structure by polarization analysis," IEEE J. Ocean. Eng. **30**, 570–587 (2005).

9. J. Liang, L. Ren, H. Ju, E. Qu, and Y. Wang, "Visibility enhancement of haze images based on a universal polarimetric imaging method," J. Appl. Phys. **116**, 1731071 (2014).

10. S. Narasimhan and S. Nayar, "Contrast restoration of weather degraded images," IEEE Trans. Pattern Anal. Mach. Intell. **25**, 713–724 (2003).

11. F. Cozman and E. Krotkov, "Depth from scattering," in *Proceedings of IEEE Conference on Computer Vision and Pattern Recognition* (IEEE, 1997), pp. 801–806.

12. C. Tsiotsios, M. Angelopoulou, T. Kim, and A. Davison, "Backscatter compensated photometric stereo with 3 sources," in *Proceedings of IEEE Conference on Computer Vision and Pattern Recognition* (IEEE, 2014), pp. 4321–4328.

13. T. Treibitz and Y. Schechner, "Turbid scene enhancement using multi-directional illumination fusion," IEEE Trans. Pattern Anal. Mach. Intell. **21**, 4662–4667 (2012).

14. N. Hautiere, J. P. Tarel, and D. Aubert, "Towards fog-free in-vehicle vision systems through contrast restoration," in *Proceedings of IEEE Conference on Computer Vision and Pattern Recognition* (IEEE, 2008), pp. 1–8.

15. J. Kopf, B. Neubert, B. Chen, M. Cohen, D. Cohen-Or, O. Deussen, M. Uyttendaele, and D. Lischinski, "Deep photo: model-based photograph enhancement and viewing," ACM Trans. Graphics **27**, 116 (2008).

16. C. Ancuti, C. O. Ancuti, T. Haber, and P. Bekaert, "Enhancing underwater images and videos by fusion," in *Proceedings of IEEE Conference on Computer Vision and Pattern Recognition* (IEEE, 2012), pp. 81–88.

17. R. Fattal, "Single image dehazing," ACM Trans. Graphics **27**, 1–8 (2008).

18. K. He, J. Sun, and X. Tang, "Single image haze removal using dark channel prior," IEEE Trans. Pattern Anal. Mach. Intell. **33**, 2341–2353 (2011).

19. P. Drews, E. Nascimento, F. Moraes, S. Botelho, and M. Campos, "Transmission estimation in underwater single images," in *Proceedings of IEEE International Conference on Computer Vision Workshops* (IEEE, 2013), pp. 825–830.

20. S. Grabtchak, T. J. Palmer, I. A. Vitkin, and W. M. Whelan, "Radiance detection of non-scattering inclusions in turbid media," Biomed. Opt. Express **3**, 3001–3011 (2012).

21. S. G. Narasimhan and S. K. Nayar, "Contrast restoration of weather degraded images," IEEE Trans. Pattern Anal. Mach. Intell. **25**, 713–724 (2003).

22. K. He, J. Sun, and X. Tang, "Guided image filtering," IEEE Trans. Pattern Anal. Mach. Intell. **35**, 1397–1409 (2013).

23. J. Y. Chiang and Y. C. Chen, "Underwater image enhancement by wavelength compensation and dehazing," IEEE Trans. Image Process. **21**, 1756–1769 (2012).

24. K. B. Gibson, D. T. Vo, and T. Q. Nguyen, "An investigation of dehazing effects on image and video coding," IEEE Trans. Image Process. **21**, 662–673 (2012).

25. R. Garcia, T. Nicosevici, and X. Cufi, "On the way to solve lighting problems in underwater imaging," in *Proceedings of IEEE Oceans* (IEEE, 2002), pp. 1018–1024.

26. J. Kim, W. Jang, J. Sim, and C. Kim, "Optimized contrast enhancement for real-time image and video dehazing," J. Vis. Commun. Image Represent. **24**, 410–425 (2013).

27. R. Fattal, "Dehazing using color-lines," ACM Trans. Graphics **34**, 13 (2014).

28. Q. Yang, S. Wang, and N. Ahuja, "Real-time specular highlight removal using bilateral filtering," in *Proceedings of European Conference on Computer Vision* (Springer, 2010), pp. 87–100.

29. C. Tomasi and R. Manduchi, "Bilateral filtering for gray and color images," in *Proceedings of the IEEE International Conference on Computer Vision* (IEEE, 1998), pp. 839–846.

30. J. Tarel and N. Hautiere, "Fast visibility restoration from a single color or gray level image," in *Proceedings of the IEEE International Conference on Computer Vision* (IEEE, 2009), pp. 2201–2208.

31. L. Yin, R. Yang, M. Gabbouj, and Y. Neuvo, "Weighted median filters: a tutorial," IEEE Trans. Circuits Syst. II **43**, 157–192 (1996).

32. Q. Yang, N. Ahuja, R. Yang, K. H. Tan, J. Davis, B. Culbertson, J. Apostolopoulos, and G. Wang, "Fusion of median and bilateral filtering for range image upsampling," IEEE Trans. Image Process. **22**, 4841–4852 (2013).

33. E. S. L. Gastal and M. M. Oliveira, "Domain transform for edge-aware image and video processing," ACM Trans. Graph. **30**, 1–8 (2011).

34. S. Yao, W. Lin, E. Ong, and Z. Lu, "Contrast signal to noise ratio for image quality assessment," in *Proceedings of International Conference on Image Processing* (IEEE, 2005), pp. 397–400.

35. Z. Wang, A. C. Bovik, H. R. Sheikh, and E. P. Simoncelli, "Image quality assessment: from error visibility to structural similarity," IEEE Trans. Image Process. **13**, 600–612 (2004).